Universidad del País Vasco/ Euskal Herriko Unibertsitatea

Faculty of Chemistry/Kimika Fakultatea

Bachelor's Degree in Chemistry

FINAL PROJECT

DEVELOPMENT OF NANOMATERIALS TO OVERCOME THE MUCOSAL BARRIER MODULATING THEIR MUCOADHESION AND MUCOPENETRATION PROPERTIES

Author: Iker Carrera Castro

Directed by: Oihane Sanz and Marcelo Calderón

Donostia-San Sebastián, September 2023

INDEX

ABSTRACT / *LABURPENA*

The aim of this work is to synthesize and develop polymeric nanoparticles (NP) that are able to interact with mucosal tissue for potential drug delivery. It is hypothesized that the NPs will be successfully functionalized giving effective nanocarriers that produce different interactions with mucus depending on the properties given by functionalization. Natural chitosan and chitosan functionalized with poly(ethylene glycol) (PEG) were used as starting reagents in different ratios to modulate nanoparticles properties regarding their solubility in aqueous medium, nanometric size, surface functionality, mucoadhesion, and mucopenetration. The NPs were characterized by Fourier-transform infrared spectroscopy (FT-IR), Nuclear magnetic resonance spectroscopy (^{1}H-NMR), Dynamic Light Scattering (DLS) and Atomic Force Microscopy (AFM).

The NPs showed stable size and polydispersity values for more than a week at room temperature and the optimized synthesis protocol, also designed throughout this work, proved to be reproducible. NP morphology was determined by AFM to be irregular and sponge-like. A PEG-chitosan derivative was successfully synthesized, which was used to produce polymeric NPs with different PEG percentage by combining commercial chitosan and the previously mentioned derivative in different proportions.

Eventually, a fluorescence quenching as a preliminary study was carried out in porcine mucin to study the interaction between the synthesized NPs and the mucus. This proved that, in fact, NPs with a higher PEG content interact less with mucin because of the mucopenetrant nature of PEG and NPs without PEG, on the other hand, interact more with mucin because of chitosan's mucoadhesive properties.

Lan honen helburua farmakoen garraio potentzialerako mukosa-ehunekin elkarreragin dezaketen nanpoartikula polimerikoak (NP) sintetizatzea eta garatzea da. Kitosano naturala eta poli(etilen glikol) (PEG)-arekin funtzionalizatutako kitosanoa erabili dira hasiera-erreaktibo gisa erlazio

desberdinetan. Horrrela, nanopartikulen propietateak modulatu nahi dira kontutan hartuz inguru akuosoan duten disolbagarritasuna, tamaina nanometrikoa, gainazal-funtzionalitatea, mukoitsasgarritasuna eta mukosarkortasuna. Nanopartikulak Espektroskopia infragorriaren Fourier transformazioa (FT-IR), Erresonantzia Magentiko Nuklearra (^{1}H-NMR), Argiaren sakabanaketa dinamikoa (DLS), eta Indar atomikoaren mikroskopia (AFM) bidez karakterizatu dira.

NP-ek tamaina eta polidispertsitate balio egonkorrak erakutsi zituzten giro tenperaturara aste bat baino gehiagoz eta sintesi-protokolo optimizatua, diseinatua proiektu honetan zehar ere, errepikagarria zela baieztatu zen. NP-morfologia irregularra eta belaki-modukoa AFM bidez determinatu zen. PEG-kitosano deribatu bat ongi sintetizatu zen, erabilia izan zena PEG ehuneko ezberdineko NPP-ak produzitzeko, kitosano komertziala eta aipatutako deribatua proportzio ezberdinetan konbinatuz.

Azkenik, quenching-fluoreszentzia proba bat egin zen txerri-muzinan sintetizatutako NP-en eta mukosaren arteko elkarrekintza aztertzeko. Honek baieztatu zuen PEG eduki handiagoa duten NP-ek gutxiago interakzionatzen dutela muzinarekin PEG-aren izaera mukosarkorrarengatik eta PEG gabeko NP-ek, aldiz, gehiago interakzionatzen dutela muzinarekin kitosanoaren propietate mukoitsaskorrengatik.

1. INTRODUCTION

1.1. MUCOSAL BARRIER

The mucosal barrier is a complex viscoelastic gel that acts as a boundary covering most of the soft tissue in the human body.[1,2] This barrier, which is essential for life, is the first line of defense against the introduction of microorganisms, foreign substances, and external pathogens into the organism.[1,2] The composition of the mucosal barrier varies in different areas of the body and consists mainly of glycoproteins and water (**Figure 1**)[4]. Glycoproteins, produced by calciform and glandular cells in the mucous epithelium, provide the characteristic viscosity and protective properties of the mucus, while water helps to mantain it in liquid state and makes its transport easier.[3]

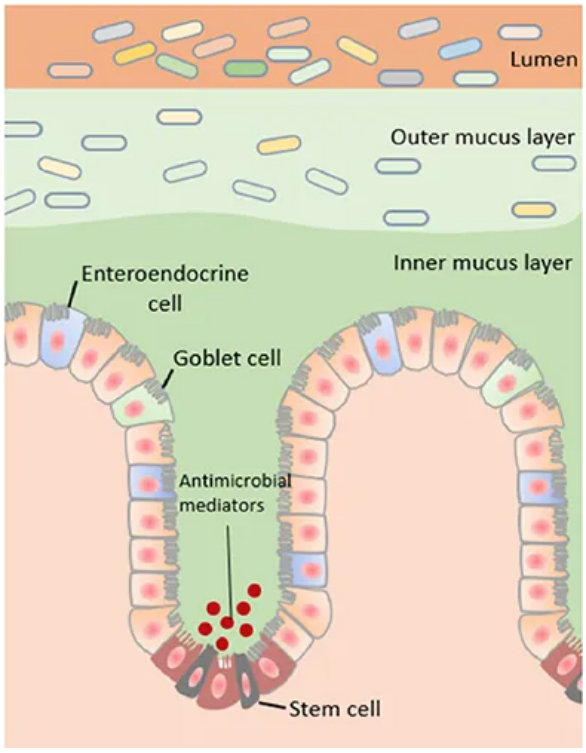

Figure 1. Structural components of the mucosal barrier.[4] This data was obtained from an open access article distributed under the terms and conditions of the Creative Commons Attribution (CC BY) license (http://creativecommons.org/licenses/by/4.0/).

One of the main functions of the mucosal barrier is to capture particles and microorganisms to prevent them from entering the organism.[5,6] The mucus acts as a sticky trap, capturing these particles and expulsing them outside of the body through mucociliary clearance (MCC) (**Figure 2**)[7]. In this process, the ciliated cells in the epithelium move the mucus in a certain direction.[5,6]

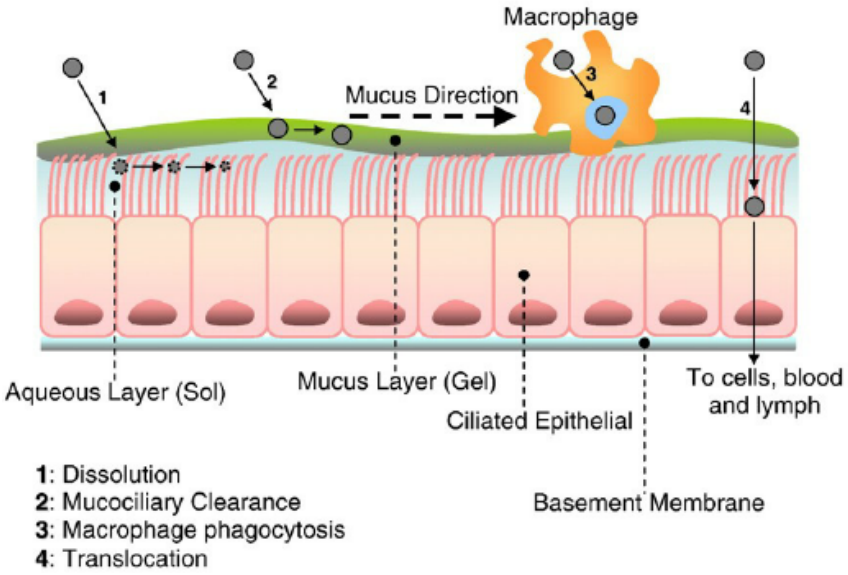

Figure 2. Mucociliary clearance mechanism.[7] (Reproduced with permission of Elsevier BV)

The mucosal barrier also plays an important role in protection against infections since the secretion and shedding mucus can easily eliminate foreign particles and pathogens that are caught in the mucus, limiting their transference to the underlying epithelial cells. However, this may represent a problem when the mucosal barrier must be overcome so therapeutics can reach the target site via oral, nasal and ocular administration routes. Mucosal barriers hamper the penetration of therapeutics into the underlying epithelial cells.[5-8] Poor mucus penetration leads to reduction of the bioavailability of therapeutics, therefore limiting their effectiveness.[8]

Moreover, some diseases, such as cystic fibrosis, asthma, or inflammatory bowel disease, directly affect the mucosal barrier. In disease conditions, such as cystic fibrosis, mucin-to-water ratio increases around 5–10 times greater than normal and mucus can reach rubber-like viscoelasticity. In these conditions the mucosal delivery of therapeutics is even more challenging.[9-11]

Therefore, the design of new carrier systems that allow to overcome the mucosal barrier represents a possibility to improve the bioavailability and effectiveness of therapeutic compounds.[1,2,8]

1.2. MUCOSAL DRUG DELIVERY

Many drug formulation technologies are being developed in order to target the mucosal barrier.[12] NP-based strategies have emerged to ease mucosal drug delivery due to the NP synthesis and modulation simplicity.[12] NPs are small organic or inorganic particles that lay in the nanoscale (0.1-1000 nm). Because of their nano-sized dimensions, NPs exhibit high surface area to volume ratio, which allows more efficient interactios with biological barriers. In addition, NPs can be easily functionalized to have different properties depending on the desired application. Some very interesting properties to modulate in NPs are mucoadhesion and mucopenetration.[12]

A substance's ability to adhere to the mucosal barrier is called mucoadhesion. Mucoadhesion is achieved through various interactions such as hydrogen bonding, disulfide linkage, electrostatic, and van der Waals interactions. Mucoadhesion process involves two phases: the contact phase and the hydration phase. The contact phase comprises the mucoadhesive particle interacting with the mucus layer, followed by the formulation spreading. Hydration phase, on the other hand, comprises the mucoadhesive particle interdiffusing or interpenetrating within the mucus. This phase is affected by the molecular mobility, molecular weight, and viscosity of the mucoadhesive particle and of the mucus. The probability of drug solubilization and absorption increases as the contact between formulation and target site increases.

Mucopenetration, on the other hand, is the ability of a substance to cross the mucosal barrier and reach the underlying epithelial cells.[13] These cells are connected by close bonds that limit the entry of substances through the mucosal barrier, especially large and hydrophopic substances.[13] A substance is more mucopenetrant when interactions with mucus are weaker or less

effective. As the substance interacts less with the matrix, in this case mucin, it does not create strong bonds that keep the substance attached to the mucin. Therefore, the substance gets through the mucus without sticking on its surface. In order to design carriers that can penetrate mucus successfully, understanding the mucus composition and properties is vital. In general, NP systems coated with different polymeric materials and muco-inert polymers have shown to be effective to penetrate the mucosal barrier.

In a few words, mucoadhesion promotes interactions with mucus for immobilization and sustained drug release, and prolongs the residence time of drugs on the mucosal barrier while avoiding premature wash-off. Mucopenetration, on the other hand, permits molecules to access the underlying epithelial tissues, diffuse through the mucus, and enhance drug uptake.[2,14]

Many strategies have been investigated to achieve mucoadhesion and mucopenetration of drug carriers, as well as solubility improvement, and drug release controlling properties.[2,15,16] The choice of strategy depends on the intended therapeutic target, the structure and composition of the mucus, and the site of absorption.

Herein, this work is aimed to synthesize a library of NPs that allows fine-tuning the NPs mucoadhesion and mucopenetration properties. For this purpose, a highly mucoadhesive polymer and a muco inert polymer were chosen to combine in different ratios to prepare different NPs samples. On one hand, chitosan was selected for NPs preparation since it is a gold standard mucoadhesive polymer.[17] On the other hand, to confer mucopenetrating properties, poly(ethylene glycol) (PEG) moieties were introduced. Since PEG with molecular weight of 5 kDa showed to be mucopenetrating,[18] we funtionalized chitosan with PEG 5 kDa to confer mucopenetrating properties to the NPs.

1.2.1. CHITOSAN

Chitosan (Ch), a natural, biodegradable, biocompatible, and bioadhesive polymer,[17] is gaining attention in the pharmaceutical fields for a wide range of drug delivery. These properties also make it an attractive material for extensive biomedical and biotechnological applications.[17-20] Chitosan is a linear polysaccharide composed of β-(1-4)-D-glucosamine and N-acetyl-D-glucosamine units (**Figure 3**). It is produced commercially by the deacetylation of chitin[17], which is the second most abundant natural biopolymer after cellulose.[17,19] The main source of chitin are the protective shells of crabs and shrimp, due to their easy exploitation. In this way, chitin residue is deacetylated into chitosan so it can be used as a chemical reagent for research and different medical therapies.[17]

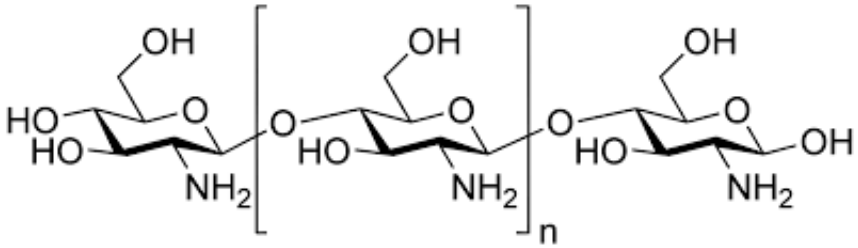

Figure 3. Chemical structure of chitosan.

Chitosan is a cationic polysaccharide that shows mucoadhesive properties and has been used to design mucoadhesive dosage forms.[19]

This polymer differs from other polysaccharides due to the presence of $-NH_2$ groups in its molecular structure, leading to the ability to form hydrogen and covalent bonds.[17,20] This allows chitosan's chemical derivatization, and also plays an important role in the solubility of chitosan macromolecules. At low pH, the amino groups undergo protonation, therefore, chitosan macromolecules become positively charged, which provides strong electrostatic interaction wtih negatively charged components of mucus layer.

1.2.2. POLY(ETHYLENE GLYCOL) (PEG)

Poly(ethylene glycol) (PEG) (**Figure 4**) is a non-toxic, non-immunogenic, and non-antigenic polymer.[21] It is highly soluble in water, European Medicines

Agency (EMA) approved GRAS (Generally Recognized as Safe) and commonly used in biomedical applications.[21] It presents both hydrophilic and net-neutrally charged surface features that avoid electrostatic and hydrophobic interactions with mucus, minimizing its adhesive interactions with mucins and making it a muco-inert polymer. [22,23] PEG avoids aggregation tendencies by steric stabilization of particles, producing formulations with increased stability during storage and application.[22,23] A slick surface can be produced by coating nanoparticles with low molecular PEG, which enables them to diffuse through mucus.[23,24] Characteristics such as PEG density and molecular weight affect mucopenetration properties of PEG-coated nanoparticles.[18]

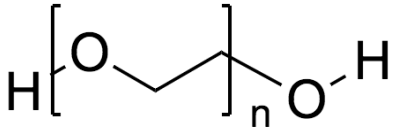

Figure 4. Chemical structure of PEG.

A high-density PEG with a relatively low molecular weight (~5 kDa) is desired in order to obtain a certain NP conformation (brush conformation) (**Figure 5**), that gives the NPs more mucopenetrant properties.[18,25] If PEG has a lower density, it tends to bend much more and becomes 'mushroom conformation', which gives it more mucoadhesive properties.[18,25,26]

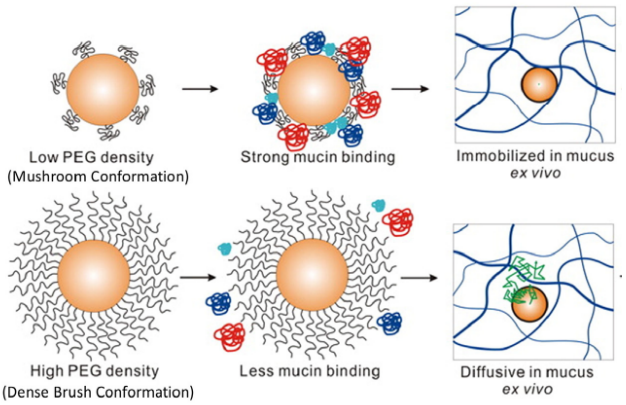

Figure 5. NP conformations varying PEG density and molecular weight.[25]
(Reproduced with permission of Elsevier BV).

In Figure 5 a comparison between low-density PEG and high-density PEG is shown. When PEG has a lower density it adopts a mushroom-like conformation, which allows strong mucin binding and therefore, a more mucoadhesive nature. On the other hand, when PEG has a higher density, a dense brush conformation is adopted and the mucin binding efficiency is weaker, which allows mucopenetration.[25]

1.3. CHITOSAN NANOPARTICLES

Chitosan NPs are polymeric NPs, which are solid colloidal particles of nanometric size produced by cross-linking reactions.[27] Chitosan cross-linking happens when it reacts with a cross-linking agent, such as dialdehydes, for instance, glutaraldehyde or formaldehyde, or polyanions like tripolyphosphate (TPP). Chitosan NPs mantain both chitosan's and NPs' properties, such as surface and interface effects or quantum size effect.[26,27] There is many ways to synthesize chitosan NPs: ionotropic gelation, microencapsulation, emulsification solvent-diffusion method, polyelectrolite complex formation, or reverse micelle method. The most developed and commonly used method is ionotropic gelation because of its simplicity regarding experimental process and the lack of organic solvent use.[28,29] It consists in the interaction of a polyanionic crosslinker, such as TPP, with chitosan's amino group.[28,29] NPs synthesized using this method usually form aggregates and have little to no stability in the long run. For this reason, it is important to optimize the chitosan NP synthesis according to each batch with a specific deacetylation degree for chitosan in order to obtain stable NPs.[28,29]

Chitosan NPs can be synthesized under magnetic stirring at room temperature using ionotropic gelation method, which is the most used method to obtain chitosan NPs. It consists of the electrostatic interaction of chitosan with polyanions. When chitosan is dissolved in acid, it becomes polycationic, exhibiting $-NH_3^+$ sites. Sodium tripolyphosphate (TPP) dissociates in water giving a negatively charged polyanion and presents both hydroxyl and phosphoric ions.[28,29] Ionic interactions can then occur between chitosan's

amino cations and negatively charged molecules and anions, such as TPP. This interaction between chitosan and TPP leads to formation of biocompatible cross-linked chitosan NPs (**Figure 6**).[28,29]

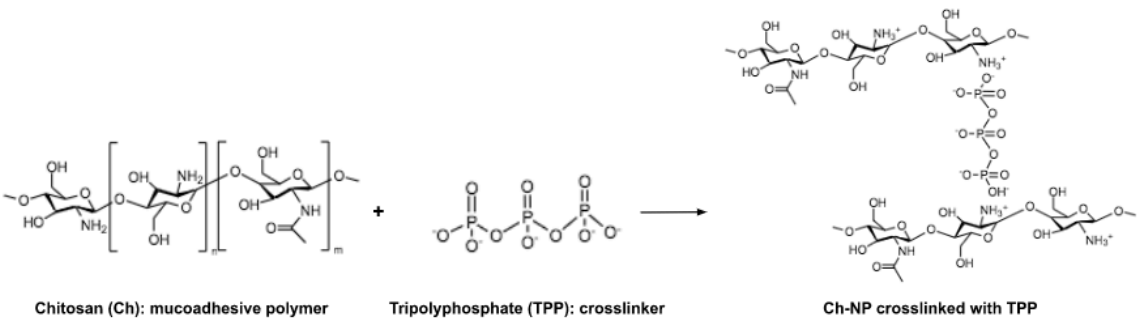

Figure 6. Ionic gelation reaction for nanoparticle synthesis.

NP size and surface charge can be modified by varying the chitosan solution concentration or the polymer:polyanion ratio.[27] Chitosan was cross-linked ionically with TPP at lower pH and by deprotonation at higher pH. [27,28]

2. OBJECTIVES

All exposed above left clear that there is a strong need of creating an effective drug delivery system for overcoming mucosal surfaces. However, as not all mucosal barriers have the same composition,[1,2] a specific drug delivery system is needed for each kind.

To achieve that, the main objective of this project is to synthesize a library of biocompatible NPs suitable for drug delivery through the mucosal barrier, modulating their mucoadhesive and mucopenetrating properties depending on the needs of the clinical application.

In order to accomplish the main objective, some specific objectives were determined:

- To improve the amount of amine groups of commercial chitosan by performing a deacetylation reaction and a fractionation process.
- To optimize the protocol of the chitosan NPs synthesis by the ionotropic gelation method, to achieve stable and reproducible nanoparticles.
- To synthesize and characterize chitosan NPs synthesized by the optimized protocol, evaluating different chitosan:TPP ratios.
- To synthesize and characterize PEGylated chitosan derivates.
- To synthesize and characterize chitosan and PEGylated chitosan NPs by the optimized ionotropic gelation method, evaluating different chitosan:chitosan-PEG ratios.
- To study the interaction of all synthesized NPs with porcine mucin by the fluorescence quenching technique.

3. EXPERIMENTAL

3.1. MATERIALS

Chitosan (Low Molecular Weight, LMW) (Sigma Aldrich), Acetic acid glacial (Reagent grade) (Scharlau), Sodium hydroxide (Synthesis grade) (Scharlau), Sodium tripolyphosphate anhydrous (EssentQ) (Scharlau), Milli-Q water (Sartorius arium mini plus), Phthalic anhydride (Merck), N,N-Dimethylformamide (99.8%, Extra Dry over Molecular Sieve, AcroSeal) (Acros Organics), Methanol (Scharlau), Methoxypolyethylene glycol acetic acid (Sigma Aldrich), 2-Bromoisobutanoic acid N-hydroxysuccinimide ester (Sigma Aldrich), 1-Hydroxybenzotriazole hydrate (Carbosynth, Scharlau), Hydrazine monohydrate (Reagent grade, 98%) (Sigma Aldrich).

3.2. CHITOSAN DEACETYLATION REACTION

The acetylation degree and molecular weight strongly affect chitosan's physicochemical properties. In this regard, a chitosan deacetylation reaction was performed to enhance its solubility and increase the number of amine groups to have more available cross-linking points during the synthesis of chitosan nanoparticles. The deacetylation reaction was performed following a protocol previously reported.[30] Firstly, chitosan was dissolved in 2 wt% acetic acid to obtain a solution with a concentration of 2 wt%. The pH of the solution was adjusted to 5.5 with a 47 wt% NaOH solution added dropwise. The solution was left to react for 1 h at 100 ºC under Ar atmosphere. Then, the solution was washed three times with Milli-Q water at 80 ºC. The obtained product, a white powder, was again resuspended in 2 wt% acetic acid and the process was repeated (**Figure 7**).[31]

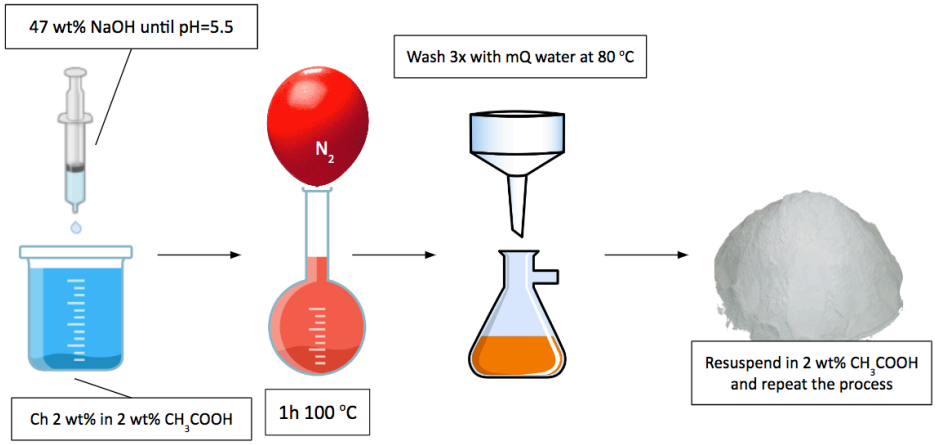

Figure 7. Scheme of the deacetylation reaction.

3.3. CHITOSAN FRACTIONATION REACTION

In order to isolate the fraction with higher deacetylation degree[35] fractionation reaction of commercial chitosan was carried out following a protocol previously reported.[34] Firstly, chitosan was dissolved in 2 wt% acetic acid to obtain a solution with a concentration of 2 wt%. A 10 wt% NaOH solution was added dropwise to adjust the pH of the solution to 5.8. The solution was vacuum filtered and the pH of the obtained liquid phase was adjusted to 7.4 using a 10 wt% NaOH solution added dropwise. The resulting solution was centrifugued at 5126 rcf for 30 min and washed three times with cold Milli-Q water before being further centrifugued at 4427 rcf for 15 min (Centrifuge, Rotina 380R, Hettich Zentrifugen). The solid phase was recovered from the centrifugue tubes and dried overnight at 40 ºC and 10 mbar in the vacuum dry oven (**Figure 8**).[34]

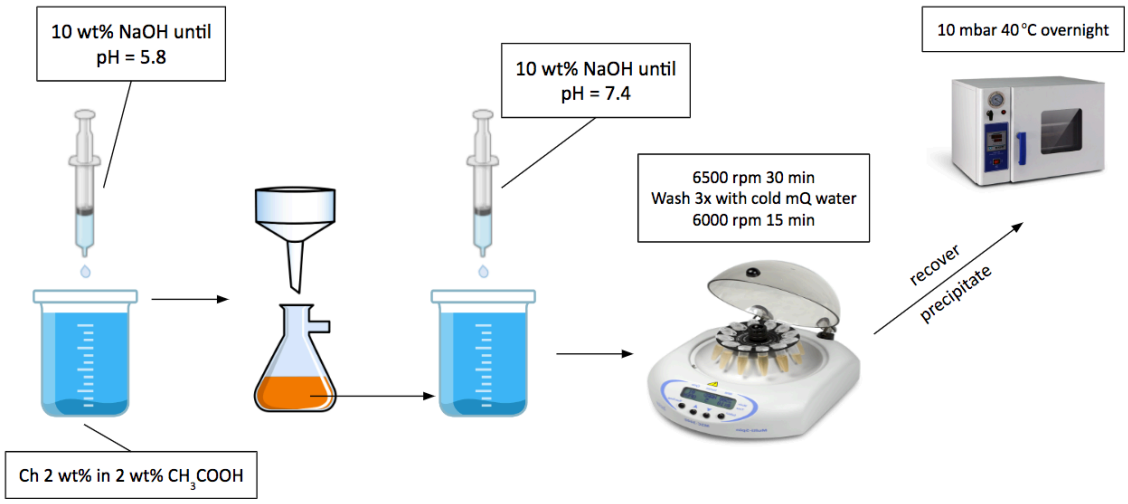

Figure 8. Scheme of the fractionation reaction.

3.4 DEACETYLATION DEGREE QUANTIFICATION

Deacetylation degree (DD) is a critical parameter of chitosan. Chitosan with a greater deacetylation degree has stronger biological effects and increased water solubility, because of a higher amino group concentration in the molecule.[30] Protonation of the $-NH_2$ functional group is vital for manifesting chitosan's biological effects and water solubility.[30,31]

Usually, the degree of acetylation of commercial chitosan is not provided by the supplier, as was in the case of the chitosan used in this work. Therefore, the deacetylation degree was quantified by FT-IR microscopy using **Equation 1**.

$$DD\ (\%) = 100 - \left(\frac{1 - \left(\frac{A_{1655}}{A_{3450}} \right)}{1.33} \cdot 100 \right) \qquad \textbf{(Equation 1)}$$

DD: deacetylation degree

A_{1655}: FT-IR spectroscopy absorbance at 1655 cm^{-1}

A_{3450}: FT-IR spectroscopy absorbance at 3450 cm^{-1}

The DD of deacetylated chitosan and fractionated chitosan was also performed to evaluate which polymer has higher DD, to be subsequently used in the NPs synthesis.

3.5. CHITOSAN-TPP NANOPARTICLE SYNTHESIS: PROTOCOL OPTIMIZATION

Chitosan NPs were synthesized using TPP as ionic cross-linker, using as staring point protocols previously reported.[34,36] The protocol was optimized in order to obtained particle in the size range of 100-300 nm with low polydispersity index. For this end, different parameters were varied (**Figure 9**).

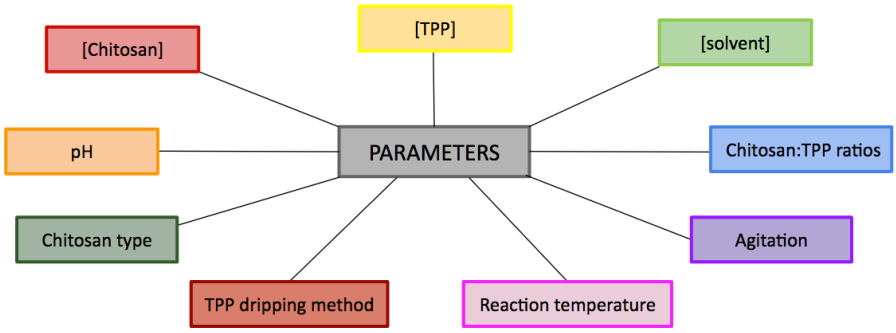

Figure 9. Parameters varied for the synthesis optimization.

Firstly, the chitosan solution was prepared, leaving dissolved the polymer in acetic acid since an acidic media is needed to solubilize chitosan in water. The acetic acid concentrations tested were 5% (v/v); 1% (v/v); 0.5% (v/v); 0.05% (v/v); 0.02% (v/v). For each solution preparation, the chitosan was left hydrated overnight at room temperature under magnetic stirring. After that, chitosan solutions were filtered using a 0.45 μm syringe filter (PES, 0.45 μm, sterile) (Fisherbrand). The chitosan concentrations tested were 3.0 mg/mL, 2.5 mg/mL, 1.5 mg/mL, 0.5 mg/mL. Before starting the reaction with TPP, the pH of the chitosan solution was adjusted to different values using a 0.5 M NaOH solution in order have the optimal amount of protonated amine groups available to react with TPP. The range of pH tested was from 2.5 to 5.5.

For the synthesis, the TPP solution in water was added to chitosan solution under magnetic strirring. Two different TPP concentrations were tested (1.0 mg/mL; 0.25 mg/mL), and also, in each case, different chitosan:TPP ratios were

considered in order to understand what happened at different crosslinker amount. The Chitosan:TPP mass ratios studied were the following: 3:1; 4:1; 5:1; 6:1; 7:1 ($m_{Chitosan}$:m_{TPP}).

In addition, the agitation values of the magnetic stirrer for the chitosan solution during the addition of TPP tested were the following: 900 rpm during the addition of TPP and 600 rpm after the whole TPP volumen was added; 600 rpm during the entire process; 500 rpm during the entire process.

Two dripping methods were tested for the TPP addition, manual dripping and mechanical dripping by syringe pump, to evaluate if the ripping method affects the final NPs size distribution.

Finally, also different temperatures were tested since there are several protocols reported in the literature that used different temperatures conditions.[34,36] The temperatures tested were the following: room temperature during the entire process; 60 ºC for the addition of TPP and then 4 ºC for the gelification time; 60 ºC for the addition of TPP and then room temperature for the gelification time.

3.6. NANOPARTICLE CHARACTERIZATION

3.6.1. DYNAMIC LIGHT SCATTERING (DLS)

The size distributions after each trial during the synthesis optimization were measured by dynamic light scattering (DLS, Malvern Zetasizer Nano ZS), (**Figure 10**). The hydrodynamic diameter (D_h) and the polydispersity index (PDI) of the nanoparticle dispersions were recorded at room temperature. An average of three measurements was taken to obtain the final values.

After the synthesis protocol optimization, the nanoparticle dispersions were measured five times to check stability of their size and polydispersity during time. The measurements were taken at the day in which the synthesis was carried out (day 0), and after 24 h (day 1), 48 h (day 2), 120 h (day 5) and 168 h (day 7).

Figure 10. Zetasizer Nano ZS.

DLS is based on the Brownian motion of dispersed particles. Particles that are dispersed in liquid move randomly in all directions and collisions occur between different particles. Particle movement is induced by an amount of energy caused by these collisions. The Stokes-Einstein equation (**Equation 2**), gives the relation between particle size and speed.[40,41]

$$D = \frac{k_B T}{6\pi\eta R_H} \qquad \textbf{(Equation 2)}$$

D: transitional diffusion coefficient.

K_b: Boltzmann constant.

T: temperature.

η: viscosity.

R_H: hydrodynamic radius.

A sample is poured into a cuvette and it is aimed with a single frequency laser, which the particles present in the sample wil scatter in all directions. The instrument detects the scattered light at a certain angle over time and the obtained signal is used to determine the transitional diffusion coefficient (D), and therefore, the particle size using Equation 2.

The incident laser light is attenuated by a gray filter placed between the laser and the cuvette to adjust the intensity of the laser to the measured sample (**Figure 11**).[42]

Theoretically, smaller particles move at higher speeds than larger particles. Larger particles, on the other hand, result in higher amplitudes between maximum and minimum scattering intensities. This intensity difference is used to generate a correlation function.[4]

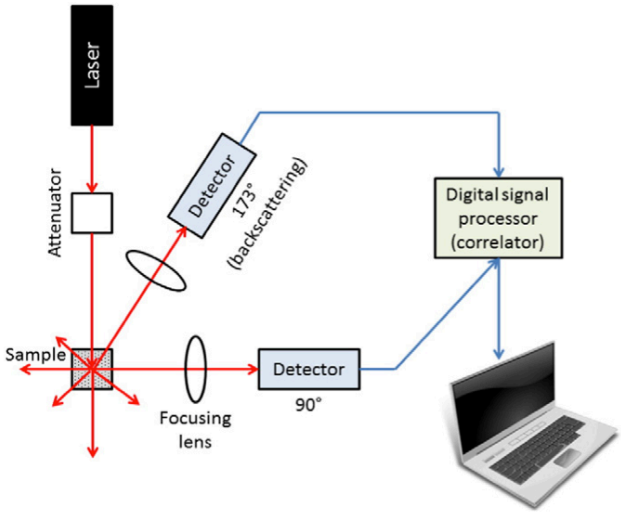

Figure 11. Schematic representation of the DLS instrumentation.[41]
(Reproduced with permission of Elsevier BV).

On the other hand, the polydispersity index (PDI) describes the broadness of the particle size distribution. However, the polydispersity index does not provide any information about the size distribution or the ratio between two particle fractions. In this work, we considered that particle size distribution with PDI below 0.3 are suitable for biomedical applications[41-43]

3.6.2. RE-DISPERSABILITY ASSAY

The ability of the synthesized NPs samples to be re-dispersed after being dried was studied. The nanoparticle dispersions obtained after the optimized synthesis were freeze-dried using a lyophilizer (Telstar LyoQuest) (**Figure 12**), to eliminate the water and to obtain a solid suitable for storage.[36,44,45]

Figure 12. Telstar LyoQuest

The dispersions were transferred to a plastic tube and freezed using liquid nitrogen. Then, the plastic tubes were put into a glass container suitable for the lyophilizer with a filter paper fixed on the top to prevent spillage of the samples. The pressure of the lyophilizer was set to 0.081 mbar and the samples were left to lyophilize for three days.

The obtained solid was weighed and a fraction of each sample was redispersed in Milli-Q water at room temperature. Finally, all redispersed samples were measured by DLS using a Zetasizer (Zetasizer Nano ZS, Malvern Instruments), (Figure 10).

The hydrodynamic diameter (D_h) and the polydispersity index (PDI) of the nanoparticle dispersions were measured at room temperature. An average of three measurements was taken to obtain the final values.

3.6.3. Proton nuclear magnetic resonance (^{1}H-NMR)

Chitosan NPs synthesized by the optimized method were characterized by ^{1}H-NMR. The nanoparticle were dispersed in deuterated water and measured by ^{1}H-NMR using a Bruker Avance 300 spectrometer (**Figure 13**). 10 scans were taken at 300 MHz for each sample to obtain the spectra. The data were analyzed using MestReNova Software.

Figure 13. Bruker Avance 300 spectrometer.

This spectroscopy is a technique used to determine the chemical structure of a substance. This is achieved by observing the magnetic field around the different proton nuclei of the substance.[40,48]

All nuclei are electrically charged and many of them have spin. When an external magnetic field is applied, an energy transfer is posible between the base energy level to a higher energy level – generally a single energy gap.[48]

The mentioned energy transfer takes place at a wavelength that corresponds to radio frequencies and when the spin returns to its base energy level, energy is emmited at the same frequency. The energy transition is dependent on the effective magnetic field at the nucleus; this field is affected by electron shielding which is dependent on the chemical environment. Consequently, it is posible to obtain information about the chemical environment from its resonant frequency.[40,54]

Chemical shift values are not precise, due to the fact that the exact value of chemical shift depends on molecular structure, solvent, temperature and the magnetic field in which the spectrum is recorded (**Table 1**).

Table 1. Chemical shift values for some functional groups.[45]

Functional group	CH_3 δ ppm	CH_2 δ ppm	CH δ ppm
CH_x-C	0.9	1.4	1.5
CH_x-C-O	1.3	1.9	2.0
CH_x-C=C	1.6	2.3	4.5-6.0
CH_x-CO	2.0	2.4	2.7
CH_x-CO-N	2.0	2.2	2.4
CH_x-N	2.4	2.5	2.8
CH_x-Ar	2.3	2.9	3.3
CH_x-O	3.3	3.6	3.9
CH_x-O-CO	3.7	4.1	-

On the other hand, the NMR spectra allow structural assingments by virtue of spin-spin coupling. The nuclei themselves possess a small magnetic field, that influence each other, changing the energy and hence frequency of nearby nuclei as they resonate and giving multiple signals according to the resonance ratio (**Table 2**).

Table 2. Adjacent protons and its coupling signals.[45]

Number of adjacent protons, n	Name	Relative intensities in splitting pattern
0	singlet	1
1	doublet	1 : 1
2	triplet	1 : 2 : 1
3	quartet	1 : 3 : 3 : 1
4	quintet	1 : 4 : 6 : 4 : 1

3.6.4. Fourier transform infrared spectroscopy

Chitosan NPs synthesized by the optimized method were characterized by FT-IR using a Bruker Alpha spectrometer (**Figure 14**). 24 scans were taken from 4000 cm^{-1} to 400 cm^{-1} with a resolution of 4 cm^{-1} for each sample to obtain the spectra.

Figure 14. Bruker Alpha spectrometer.

IR spectroscopy is a research tool that was significantly improved by the introduction of Fourier transform techniques.[49]

FT-IR spectroscopy is a microspectroscopic technique that provides information on molecular structure with great microscopic resolution. Microscopic samples can be analyzed directly, in air, at room temperature and pressure, wet or dry. This technique is also non-destructive and in many cases the sample is not wasted.[50]

Both qualitative and quantitative information can be obtained using FT-IR, and a wide range of organic compunds and functional groups can be identified by their unique pattern of absorption (**Table 3**).[50,51]

Table 3. FT-IR absorption values for some functional groups.[51]

Functional group	Wavenumber (cm^{-1})	Absorption intensity
Alkane (C-H)	2850-2975	Medium to strong
Alcohol (O-H)	3400-3700	Strong, broad
Alkene (C=H)	1640-1680	Weak to medium
(C=C-H)	3020-3100	Medium
Alkyne (C≡C)	2100-2250	Medium
(C≡C-H)	3300	Strong
Nitrile (CN)	2200-2250	Medium
Aromatics	1650-2000	Weak
Amines (N-H)	3300-3350	Medium
Carbonyls (C=O)		
Aldehyde (CHO)	1720-1740	
Ketone (RCOR')	1715	Strong
Ester (RCOOR')	1735-1750	
Acid (RCOOH)	1700-1725	

FT-IR has many advantages over dispersive infrared spectroscopy, such as high energy throughput, speed, computer assisted spectral processing, multiscanning capability, and computer storage of spectra.[52]

One of the most widely used spectral processing operations is the digital subtraction of absorbance spectra in order to reveal small differences between two materials.[51,52]

FT-IR has become a powerful tool for biological system studies at molecular level. Since the initial demonstration of the practicality of digital removal of interfering water absorption bands in a number of biopolymer solutions, the scope of FT-IR research in biopolymers has been steadily expanding.[53]

3.6.5. Atomic Force Microscopy (AFM) spectroscopy

The morphology of the chitosan NPs synthesized by the optimized method were syudied by Atomic Force Microscopy (AFM). The measurements were performed on AFM Dimension ICON (Bruker) (**Figure 15**) equipped with a cantilever ScanAsyst (Bruker) (70 kHz, 0.4 N/m) at room temperature in PeakForce Tapping mode. The substrate was mounted on a magnetic platform, and followed by the PeakForce Tapping scanning with 512 points per line and a rate of 0.9 Hz. Image analysis was programmed by NanoScope Analysis. All the images should be flattened in 3rd order to correct the defect generated by the scanning process.

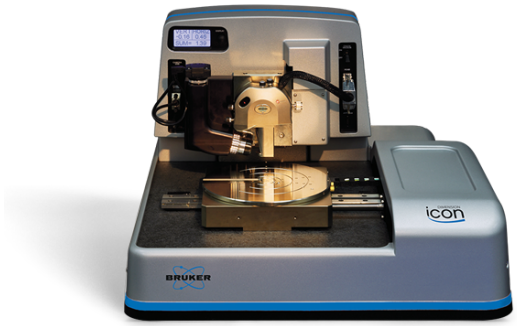

Figure 15. AFM Dimension ICON.

AFM spectroscopy is an atomic microscopy technique that uses force-distance curves to produce high definition images that are a useful tool for studying surface interactions.[54]

This technique allows the inspection and superficial characterization of both organic and inorganic materials, offering morphological information of the analyzed material.[54] Moreover, both wet and dry samples are suitable for this microscopy technique. Atomic interactions are measured to produce an image and different kinds of signals generated from the sample are produced by this apparatus and are used to inspect many morphological characteristics of microscopic areas.

This technique was used for the processing and analysis of microscopic images, to describe and compare the morphological characteristics of the nanoparticle dispersions.[54]

3.7. SYNTHESIS OF PEGYLATED CHITOSAN

Chitosan was functionalized with methoxypolyethylene glycol, both mentioned in section 4.1., in order to confer mucopenetrant properties to the NPs synthesized with the resulting chitosan-PEG. The functionalization was achieved by following the below mentioned procedure.[38,39]

Firstly, 100 mg of chitosan were put together with 1.86 mmol of phthalic anhydride in DMF at 120 ^{o}C, 8 h under Ar atmosphere. The resulting solution was put in an ice bath, vacuum filtered and washed with methanol. The precipitate was dried until a yellowish powder was obtained. Then, 0.24 mmol of PEG-COOH, 0.12 mmol of EDC and 0.19 mmol of HOBt were mixed in 1.4 mL of 17.22 wt% DMF at room temperature. After 30 min, 20 mg of the yellowish powder obtained in the previous step were added to the mixture and left to react overnight at 60 ^{o}C. Then, the solution was washed with ethanol three times and put to dialyze against distilled water. After 3 days of dialysis, the product was lyophilized and 80 mg of it were mixed with 0.4 mL of hydrazine monohydrate and 0.3 mL of DMF at 100 ^{o}C during 2h. The solution was further dialyzed. Eventually, after 34 days of dialysis against distilled water, the solution was lyophilized again to give the desired product, mPEG-OC. (**Figure 16**).[38,39] After each synthetic step, the porducts were characterizeb by FT-IR and ^{1}H-NMR to confirm the products formation.

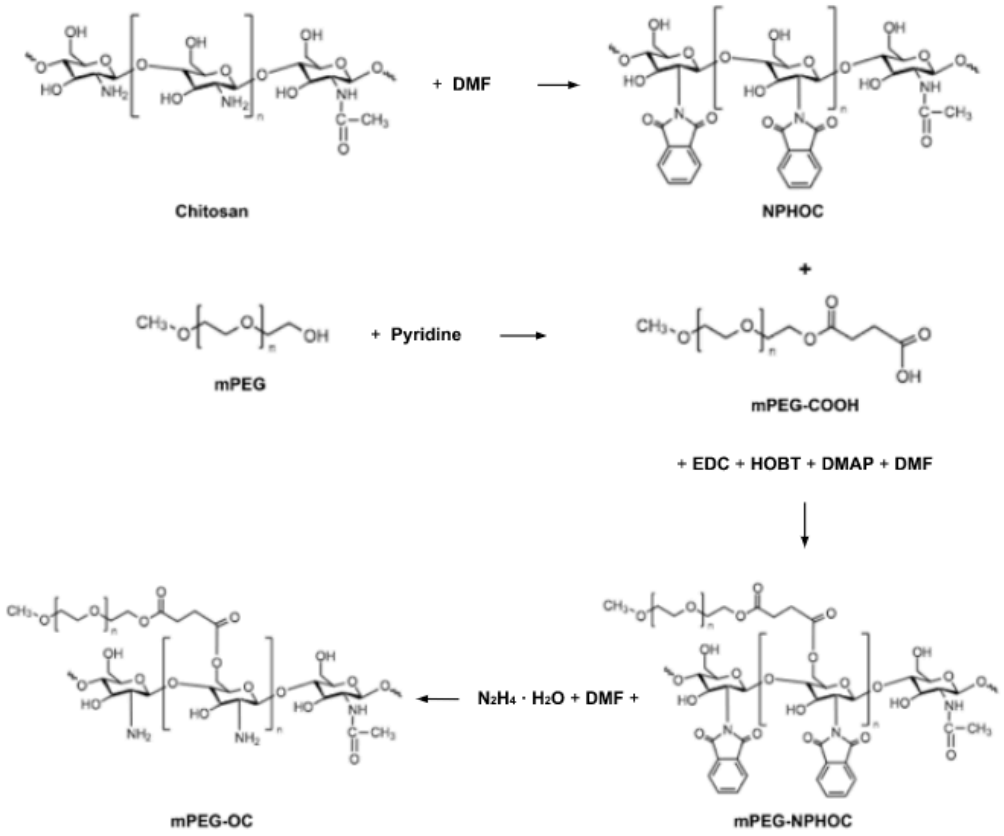

Figure 16. Scheme of the chitosan-PEG synthesis.

3.8. SYNTHESIS OF PEGYLATED CHITOSAN NANOPARTICLES

Chitosan was functionalized with methoxypolyethylene glycol in order to confer mucopenetrant properties to the NPs. The optimized synthesis protocol was performed at one selected polymer TPP ratio, using a mixture of chitosan and PEG-chitosan. The mass ratios of chitosan:chitosan-PEG studied were: 100:0; 75:25; 50:50; 25:75.

The final NPs obtained were characterized by DLS, ^{1}H-NMR, FT-IR, and AFM.

3.9. NANOPARTICLE-MUCIN INTERACTION STUDIES BY FLUORESCENCE QUENCHING TECHNIQUE

Mucin shows an intensive fluorescence at about 360 nm, upon excitation at 258 nm. If mucin is incubated with NPs, the mucin fluorescence spectra changes if there are interactions between them. The fluorescence intensity decreases, a phenomenon that is called fluorescence quenching. In order to study how is the interaction of all NPs synthesized with mucin, the quenching assay was performed as follows. Fluorescence spectra of mucin (0.1 mg/mL) in prescense of different NPs concentration (1.000; 0.500; 0.250; 0,125; 0.063; 0.031; 0.016 mg/mL) were recorded using a multimode Plate Reader SYNERGY neo2, Biotek (**Figure 17**). The samples were measured using a Greiner 96 Black Flat Bottom Fluotrac plate. The emission spectra were recorded in the range of 300-700 nm after excitation at 258 nm.[56]

Figure 17. Plate Reader SYNERGY neo2.

Negative controls including the NPs without mucin were performed, since chitosan also can present fluorescence at these experimental conditions. From the negative controls, one NP concentration was selected, and from emission intensities obtained at this concentration, the changes in the fluorescence intensity were calculated as shown in **Equation 3**:

$$\Delta F = F_0 - F \qquad \textbf{(Equation 3)}$$

ΔF: fluorescence intensity difference.

F_0: fluorescence intensity of mucin alone.

F: fluorescence intensity together with quencher concentration.

4. RESULTS AND DISCUSSION

4.1. DEACETYLATION REACTION AND FRACTIONATION PROCESS

The degree of deacetylation of commercial chitosan, and the products from the deacetylation reaction and the fractionation process were quantified. The three samples were characterized by FT-IR to determine their degree of deacetylation and therefore, choose the chitosan with the highest deacetylation degree to synthesize the polymeric nanoparticles. A higher deacetylation degree indicates a higher NH_2 content and therefore, a greater solubility, to enhance the amount of polymer that can be solubilized to perform the reaction. Also the increase of degree of deacetylation provides more functional points to perform the crosslinking reaction. **Figure 18** shows the FT-IR spectra for commercial chitosan, deacetylated chitosan and fractionated chitosan.

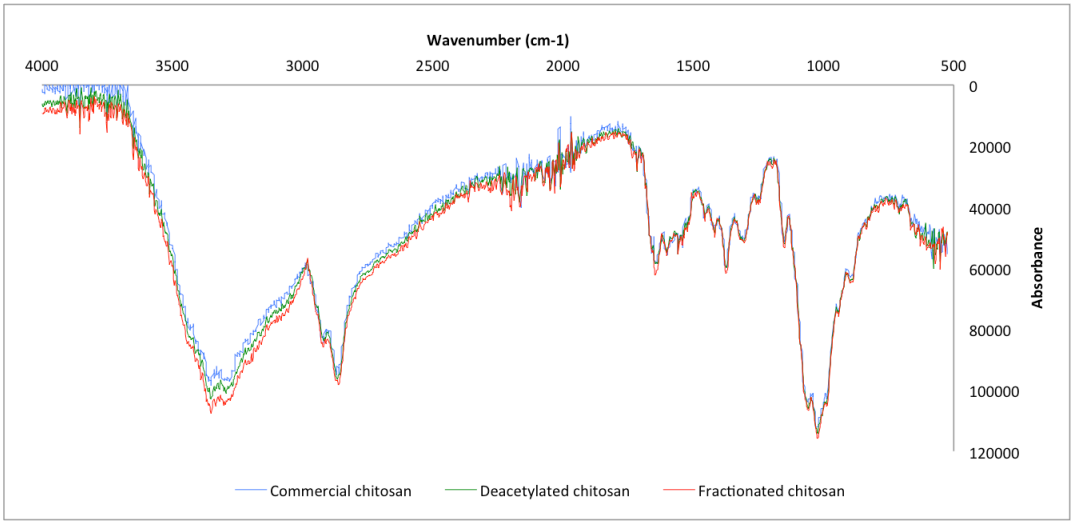

Figure 18. FT-IR spectra for chitosan.

As shown in Figure 18, there are four main peaks in the spectra that give valuable information about the chemical structure of the different chitosans. The broad peak around 3300 cm^{-1} corresponds with the –OH functional group; the peak around 2900 cm^{-1} belongs to the alcanes forming the glucose cycles; the signal that spreads between 1300 and 1700 cm^{-1} is given by the $–NH_2$ group and the large peak around 1000 cm^{-1} belongs to the –O- functional group that links the glucosamine rings.

The degree of deacetylation of each kind of chitosan can easily be calculated by using Equation 1.

The degree of deacetylation for the commercial chitosan was of 75.84%, which is a bit higher than what was expected. The degree of deacetylation was calculated to be of 77.26% for the deacetylated chitosan and of 79.23% for the fractionated chitosan.

The difference between the deacetylation degrees of the three chitosans was not so different, so the commercial chitosan was further used for the synthesis of the chitosan NPs.

4.2. OPTIMIZATION OF THE CHITOSAN-TPP NANOPARTICLE SYNTHESIS

The optimization of the Chitosan-TPP NP synthesis was carried out by altering different parameters (Figure 9) and performing the synthesis changing only one parameter at a time. After many trials, these were the conditions that produced the target NPs (a hydrodynamic diameter between 100 and 300 nm and a polydispersity index below 0.300):

- Chitosan solution concentration: 2.5 mg/mL.
- TPP solution concentration: 0.25 mg/mL.
- Solvent concentration: 0.05% (v/v).
- $m_{chitosan}$:m_{TPP} ratio: 5:1.
- pH: 5.5.
- Agitation: 500 rpm.
- Temperature: room temperature.

- TPP dripping method: mechanical dripping by syringe pump.

These choices were made after confirming that by using those exact conditions the target NPs were obtained. The rest of conditions tested produced NP dispersions with a very high polydispersity index or NPs with a hydrodynamic diameter aboved the desired value. The optimized protocol with all the chosen conditions is represented in **Figure 19**.

The synthesis of chitosan NPs was performed by adaptation of a previously reported protocol.[36] Chitosan was dissolved in 5% (v/v) acetic acid to obtain a solution with a concentration of 2.5 mg/mL and this was left to stir for 24 h. A 0.5 M NaOH solution was used to adjust the pH of the chitosan solution before being passed through a 0.45 μm syringe filter (PES, 0.45 μm, sterile) (Fisherbrand). Then, a 0.25 mg/mL TPP solution was prepared in mQ water. In order to get the desired Chitosan:TPP ratios, the calculated TPP volumes were added to diluted chitosan solutions dropwise by using the syringe pump (New Era Pump Systems, Inc.) at a rate of 0.3 mL/min with an agitation of 500 rpm at room temperature (Magnetic stirrer, OVAN). When the TPP was poured in completely, the solutions were left to react for 30 min. After that, the solutions were centrifuged at 2744 rcf, 15 min and the liquid phase was recovered (Centrifuge, Rotina 380R, Hettich Zentrifugen). Eventually, the solutions were analyzed by DLS to measure the hydrodynamic diameter of the NPs (DLS, Malvern Zetasizer Nano ZS) (Figure 19).[36,37]

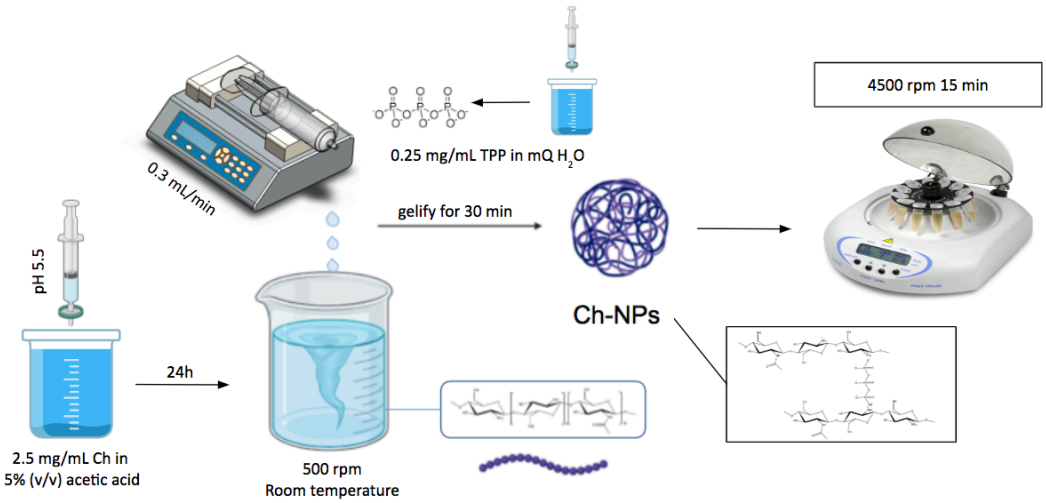

Figure 19. Scheme of the nanoparticle synthesis.

4.3. CHITOSAN-TPP NANOPARTICLE CHARACTERIZATION

The chitosan-TPP NPs synthesized were characterized by DLS. The NP size and polydispersity index were periodically measured for a week at room temperature to check the stability and reproducibility of the synthesized NP dispersions.

In **Figure 20** the stability measurements of both the hydrodynamic diameter and the polydispersity index of the nanoparticle dispersions for the 5:1 ($m_{Chitosan}$:m_{TPP}) ratio are shown.

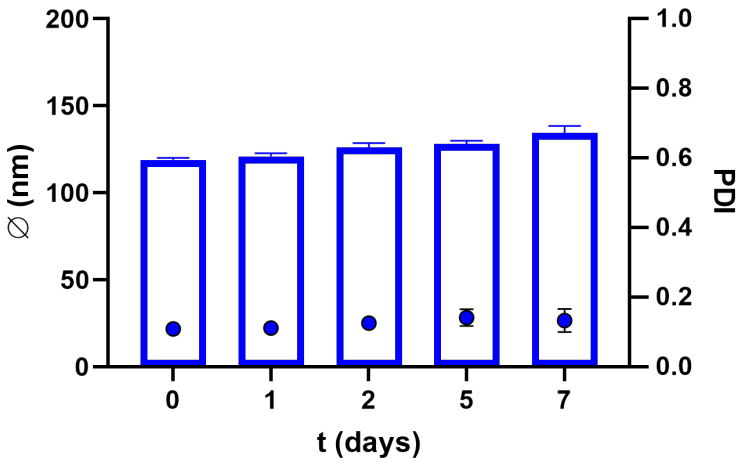

Figure 20. Nanoparticle hydrodynamic diameter and polydispersity stability in time.

As observed in Figure 20, both the hydrodynamic diameter and the polydispersity index of the synthesized nanoparticles remain stable for more than a week at room temperature for the 5:1 ($m_{Chitosan}$:m_{TPP}) ratio.

Three independent batches of 5:1 ($m_{Chitosan}$:m_{TPP}) polymeric nanoparticles were produced, following the optimized synthesis procedure described in section 4.2. were measured to check if the optimized protocol was reproducible. Indeed, the results showed that the optimized protocol for the NPs synthesis was reproducible and that the produced NPs remain stable for more than a week at room temperature with a hydrodynamic diameter of 139 ± 4 nm and a polydispersity index of 0.13 ± 0.02.

A redispersability study also was perfomed to evaluate if the NPs can be redispersed after being dried. The samples were dried by lyophylization and the size distributions were checked after lyophilization and redispersion in water. **Figure 21** shows the size and polydispersity values measured before and after the nanoparticle dispersions (5:1 ($m_{Chitosan}$:m_{TPP}) ratio) were freeze-dried and resuspended in water.

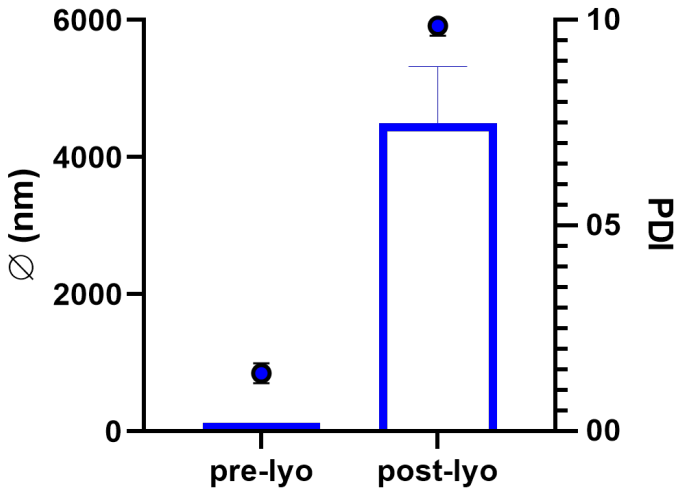

Figure 21. Lyophilization and resuspension effect in the size and polydispersity of the nanoparticles.

Figure 21 shows that the NPs dispersions lost their original size and polydispersity values after being freeze-dried. This indicates that after freeze-drying, the NPs interact so strongly between themselves that it is impossible to redisperse in water properly. In the future, new strategies incorporating extra excipients should be explored to solve this issue.

In addition, the NPs obtained were analyzed by FT-IR. **Figure 22** shows the FT-IR for the 5:1 ($m_{Chitosan}$:m_{TPP}) ratio NPs prepared using the optimized synthesis protocol.

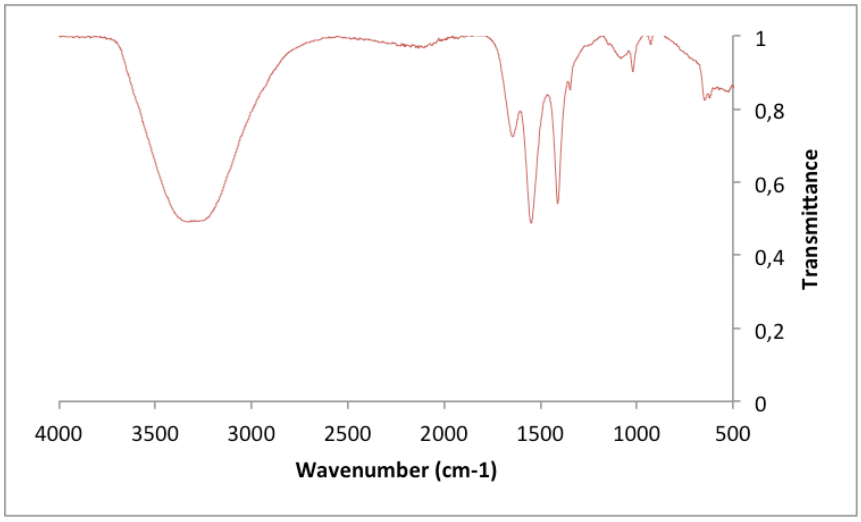

Figure 22. Ch-TPP NPs (5:1) FT-IR spectra.

As shown in Figure 22, the main peaks for Chitosan-TPP NPs are the broad peak between 3500 and 3000 cm^{-1} belonging to the –OH functional group and the sharp peaks around 1500 cm^{-1} belonging to the –O- functional groups of TPP that link the polymeric chains between them.

The obtained NPs were also analyzed by AFM. **Figure 23** shows the AFM spectra for the Chitosan NPs synthesized by the optimized protocol at 5:1 ($m_{Chitosan}$:m_{TPP}) ratio.

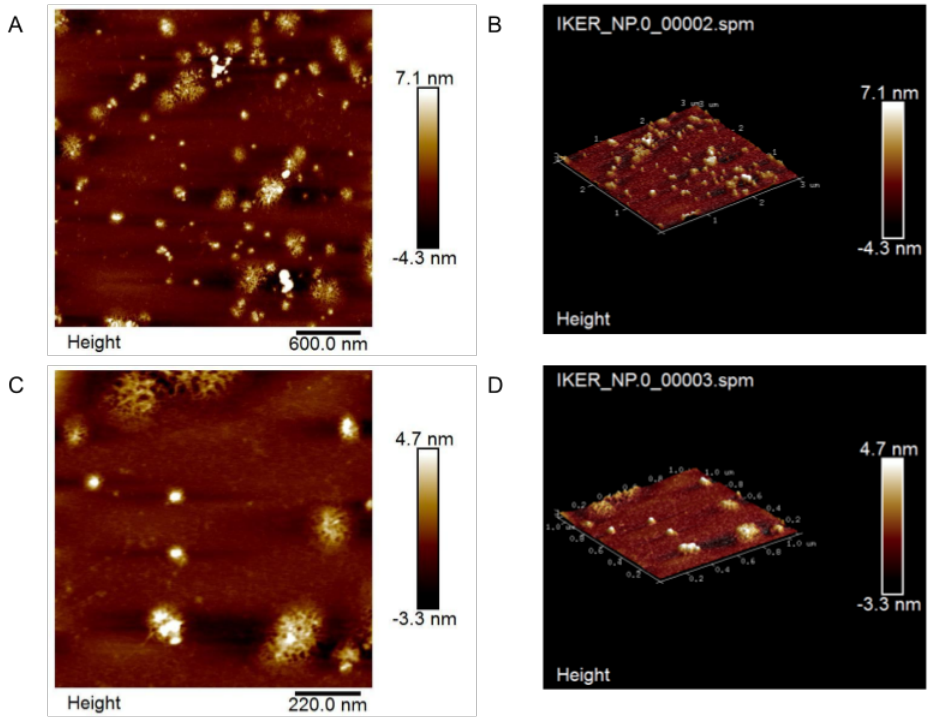

Figure 23. Ch-TPP NPs (5:1) AFM image. (a) 7 micron grain analysis image in 2D, (b) 7 micron grain analysis image in 3D, (c) 5 micron grain analysis image in 2D and (d) 5 micron grain analysis image in 3D.

AFM images show that synthesized Chitosan-TPP NPs exhibit nanosponge-like morphology; they look wrinkled and uneven. In fact, also some aggregates are evident from the figure 23A. This can be due to the interaction between NPs. It is important to highlight that at experiment conditions the sample is dried. So, the aggregates observed here are in agreement with the behavior of NPs in the redispersability test.

4.4. CHITOSAN-PEG CHARACTERIZATION

The chitosan-PEG characterization was tracked by analyzing the intermediate products obtained during the synthesis using FT-IR and ^{1}H-NMR.

Figure 24 shows the FT-IR spectra for the products obtained during the synthesis of chitosan-PEG: NPHOC, mPEG NPHOC, and mPEG-OC.

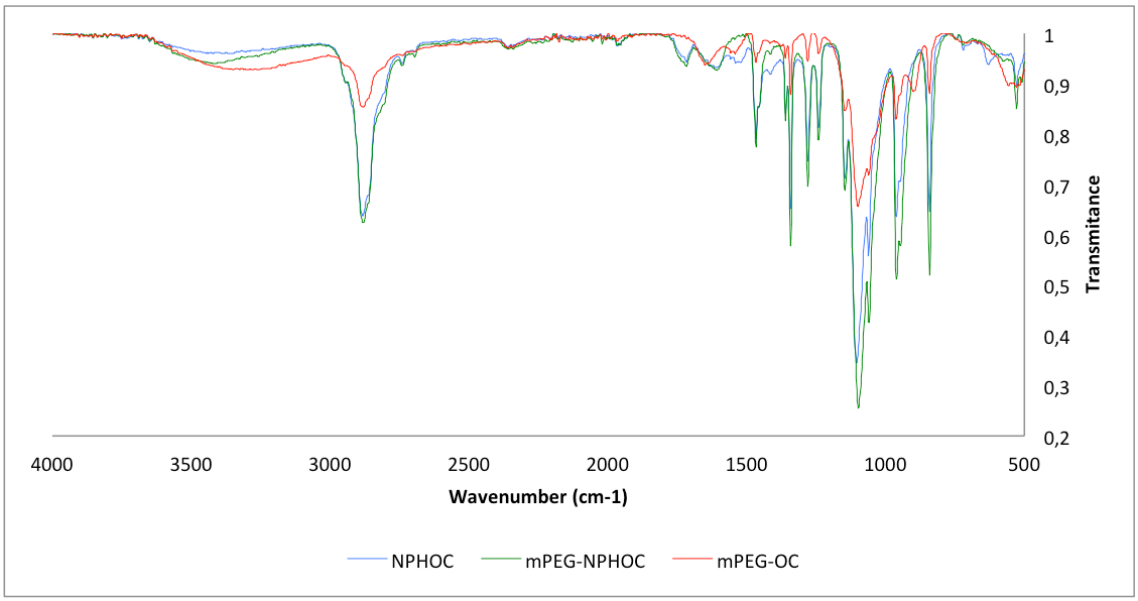

Figure 24. FT-IR spectra for Chitosan-PEG synthesis products.

In Figure 24, the progression of the products obtained in the Chitosan-PEG synthesis is shown. The peak around 3000 cm^{-1}, which belongs to the tertiary amines present in the N-aromatic cycles, is present for both NPHOC and mPEG-NPHOC but not for the final product, which comes together with the molecules shown in Figure 13. The peak around 1000 cm^{-1}, which belongs to the –O- functional group, is more intense for the first two products in comparison with the third one. This allows to conclude that chitosan functionalization successfully occurred.

Figure 25 shows the ^{1}H-NMR spectra for the products obtained during the synthesis of Chitosan-PEG: NPHOC, mPEG NPHOC, and mPEG-OC.

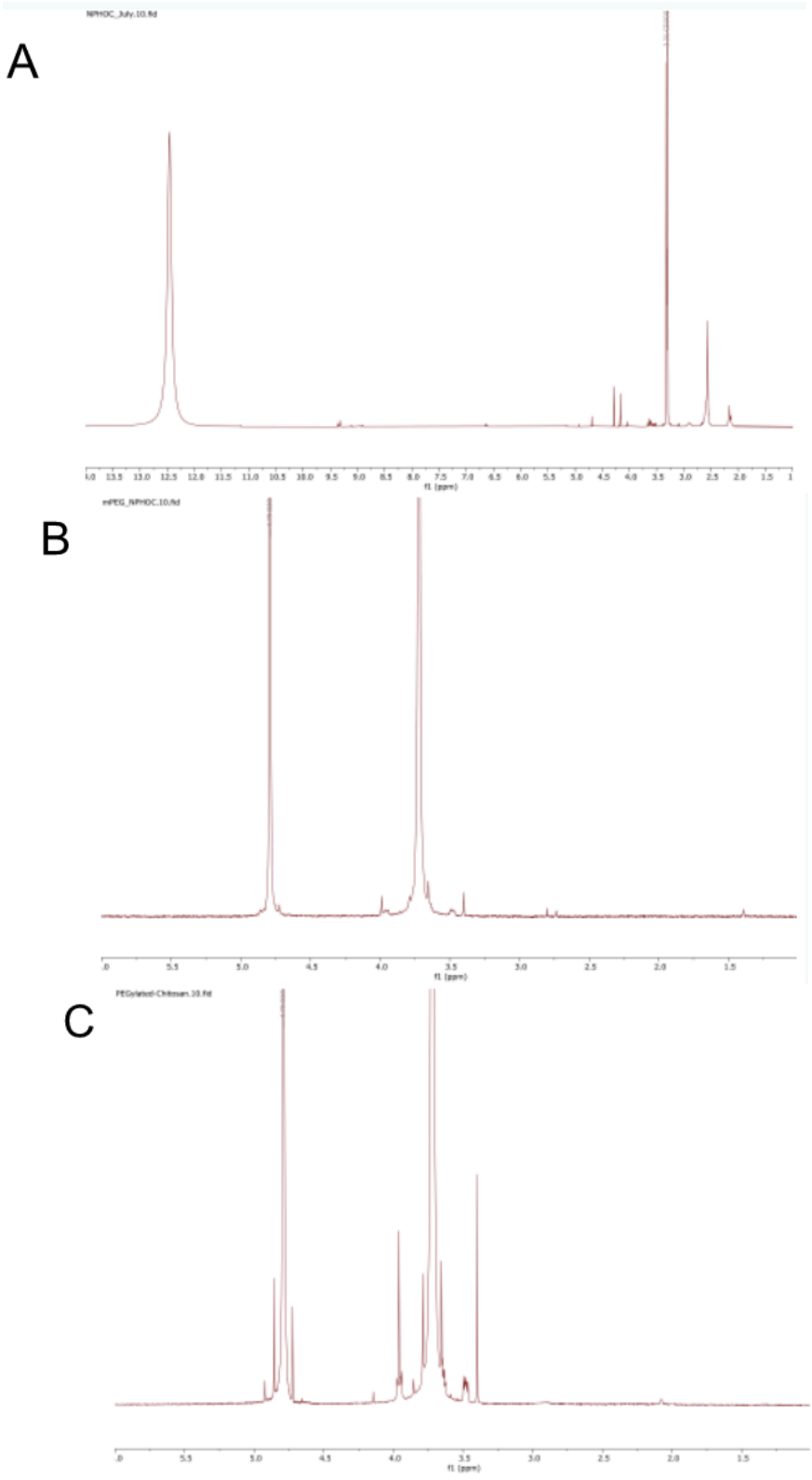

Figure 25. 1H-NMR spectra for Chitosan-PEG synthesis products; (a) NPHOC; (b) mPEG-NPHOC; (c) mPEG-OC.

In Figure 25, the progression of the products obtained in the Chitosan-PEG synthesis is shown, which allows to conclude that chitosan functionalization successfully occurred. Figures 25 (b) and 25 (c) show the characteristic peaks for PEG around 3.5 and 5.0 ppm, corresponding to the protons of the hydroxyl groups present in PEG.

4.5. PEG-CHITOSAN NANOPARTICLE SYNTHESIS

After successful optimization of the synthesis protocol with Chitosan NPs using the commercial chitosan, NPs were synthesized at 5:1 ($m_{Chitosan}$:m_{TPP}) ratio, with different chitosan:PEG-chitosan ratios in order to obtained different NPs that allows modulating the interaction of NPs with mucusal barrier.

In Figure 26 shows the hydrodynamic diameter and the polydispersity index for all synthesized PEGylated chitosan NPs using different at different time in order to evaluate the stability of the samples during the time.

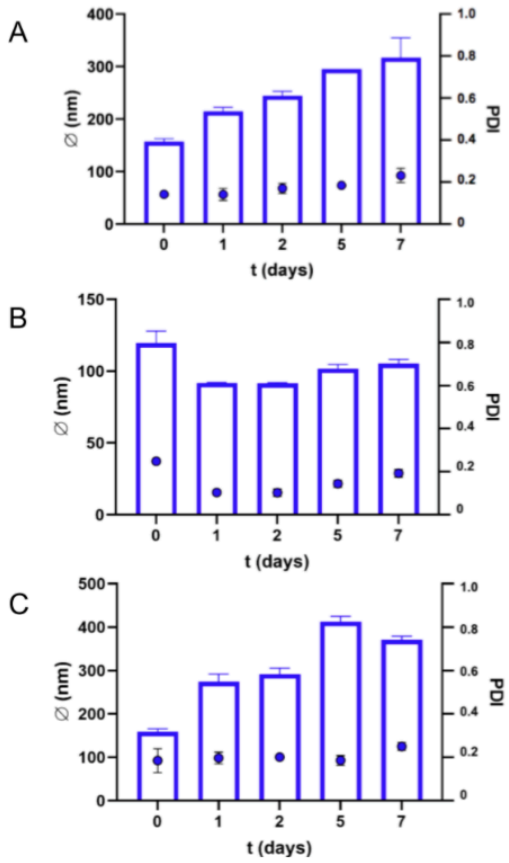

Figure 26. Nanoparticle hydrodynamic diameter and polydispersity stability in time for the (a) 75:25, (b) 50:50 and (c) 25:75 (Chitosan %:Chitosan-PEG %) ratios.

As observed in **Figure 26**, both the hydrodynamic diameter and the polydispersity index of the synthesized nanoparticles remain stable for more than a week at room temperature for all chitosan:chitosan-PEG ratios.

In addition, PEGylated chitosan NPs were characterized by FT-IR (**Figure 27**).

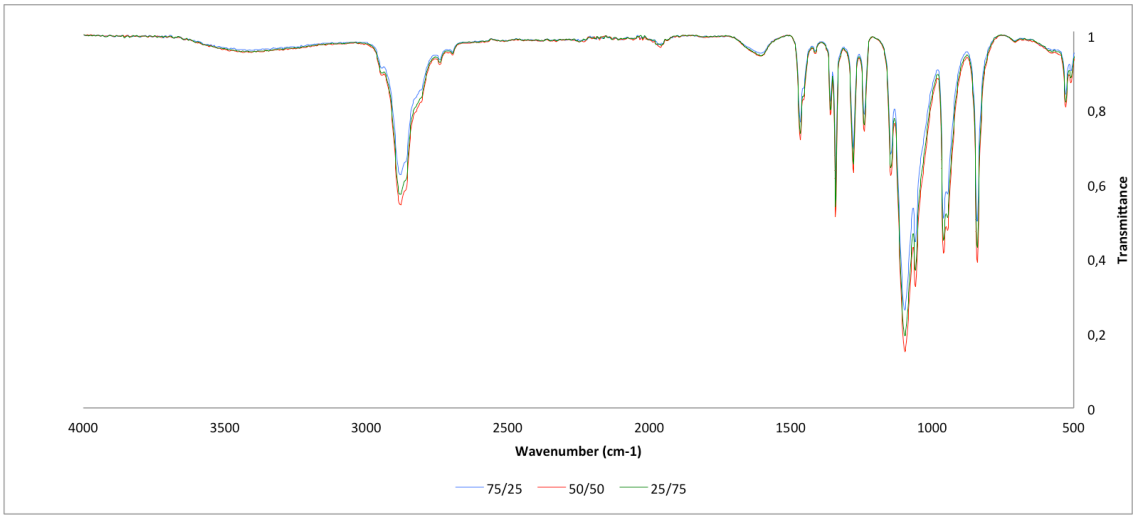

Figure 27. FT-IR spectra for the 75:25, 50:50 and 25:75 (Chitosan %:Chitosan-PEG %) ratios.

As shown in **Figure 27**, the main peaks for the 75:25, 50:50 and 25:75 (Chitosan%:Chitosan-PEG %) ratio NPs are the peak between 3500 and 3000 cm^{-1} belonging to the –OH functional group and the sharp peaks around 1000 and 1500 cm^{-1} belonging to the –O- functional groups of TPP that link the polymeric chains between them.

4.6. FLUORESCENCE QUENCHING STUDY

Figure 28 shows the results for the preliminary test performed to check the fluorescence quenching of the nanogels, and therefore the interaction between the synthesized polymeric NPs and mucin.

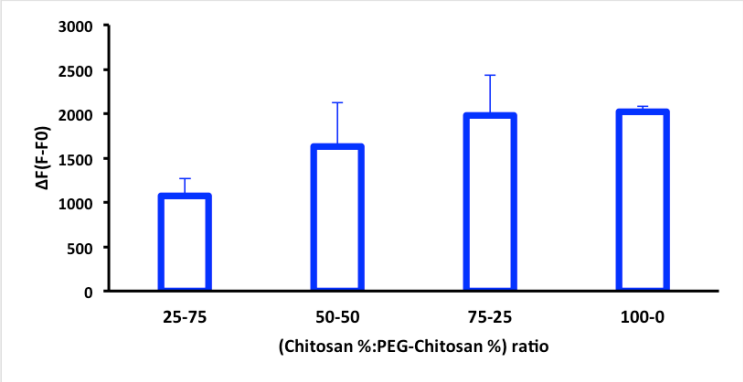

Figure 28. Fluorescence quenching results for the 0.25 mg/mL NP concentration at different Chitosan %:Chitosan-PEG % ratios.

As shown in Figure 28, as the NPs PEG content increases, the fluorescence quenching of the batch decreases, which indicates lesser interaction of the NPs with the mucin and therefore, less mucoadhesive and more mucopenetrant behaviour, which is expected due to the composition of the NPs (less natural chitosan percentage indicates less mucoadhesive behaviour). Therefore, it is proven that adding PEG to chitosan and combining commercial and derivative chitosan for the synthesis of NPs does, in fact, allow the modulation of their properties and consequently, the interaction of the mentioned NPs with mucus.

Although, this is a proof of concept and a preliminary study to see an approximation of how the composition of the NPs affects the interaction they have with mucin. Further investigation on this area would conclude in a more complete analysis of the interaction of the NPs with mucose carrying out more ***in vitro*** experiments.

5. CONCLUSIONS / *ONDORIOAK*

In this work, a natural polymer with mucoadhesive properties, chitosan, was successfully functionalized with another polymer with mucopenetrant properties, poly(ethylene glycol). Chitosan's nature was altered and presented the possibility of mixing functionalized and non-functionalized chitosan in different proportions to synthesize nanoparticles that would be able to face different mucosal barriers efficiently and be applicable for various clinical practices.

An optimized protocol for the synthesis of the above mentioned nanocarriers was also successfully developed, producing nanoparticle dispersions of the desired size and polydispersity. The protocol also proved to be reproducible.

Indeed, four different ratios of functionalized and non-functionalized chitosan were mixed to produce nanocarriers with different properties regarding mucoadhesion and mucopenetration, all of which were confirmed by characterization via spectroscopic techniques. All four ratios gave nanoparticle dispersions that showed size and polydispersity stability in time at room temperature.

A preliminary study regarding fluorescence quenching was successfully carried out in porcine mucin, confirming that NPs with a higher PEG content interact less with mucin because of the mucopenetrant nature of PEG and NPs without PEG, on the other hand, interact more with mucin because of chitosan's mucoadhesive properties. Therefore, adding PEG to chitosan and combining commercial and derivative chitosan for the synthesis of NPs does, in fact, allow modulation of their properties and consequently, the interaction of the mentioned NPs with mucus.

Lan honetan, propietate mukoitsaskorrak dituen polimero natural bat, kitosanoa, propietate mukosarkorrak beste polimero batekin, poli(etilen glikol)-a, funtzionalizatu da arrakastasuki. Bere izaera aldatzeko eta proportzio ezberdinetan kitosano funtzionalizatu eta ez-funtzionalizatua nahasteko aukera eskaintzeko, horrela mukosa mintz desberdinak

eraginkorki gainditu dezaketen nanopartikulak sintetizatzeko eta ondorioz, praktika kliniko askotan aplikagarriak izan daitezen lortu da.

Aipatutako nanogarraiatzaileak sintetizatzeko protokolo optimizatu bat garatu da ere, desiratutako tamaina eta polidispertsitatea duten nanopartikula dispertsioak emanez.

Hain zuzen ere, kitosano funtzionalizatu eta ez-funtzionalizatu lau proportzio ezberdin nahastu dira propietate desberdinetako nanogarraiatzaileak emateko, mukoitsasgarritasunari eta mukosarkortasunari dagokionez, zeinak teknika espektroskopikoen bidezko karakteriazioarekin konfirmatu diren. Lau proportzioek giro-tenperaturan tamainan eta polidispertsitatean egonkortasuna aurkeztu zuten nanopartikula dispertsioak eman zituzten.

"Quenching"-fluoreszentzia aurretiko proba bat egin zen txerri-muzinan, PEG eduki handiagoa duten NP-ek gutxiago interakzionatzen dutela muzinarekin PEG-aren izaera mukosarkorrarengatik eta PEG gabeko NP-ek, aldiz, gehiago interakzionatzen dutela muzinarekin kitosanoaren propietate mukoitsaskorrengatik. Beraz, kitosanoari PEG gehitzea eta kitosano komertzial eta deribatua konbinatzea NP-en sintesirako hauen propietateen eta ondorioz, hauen eta mukosaren arteko elkarrekintzaren modulazioa ahalbidetzen du.

6. BIBLIOGRAPHY

(1) France, M. M., & Turner, J. R. (2017). The mucosal barrier at a glance. ***Journal of Cell Science***, ***130***(2), 307–314.

(2) Watchorn, J., Clasky, A. J., Prakash, G., Johnston, I. A. E., Chen, P. Z., & Gu, F. X. (2022). Untangling Mucosal Drug Delivery: Engineering, Designing, and Testing Nanoparticles to Overcome the Mucus Barrier. In ***ACS Biomaterials Science and Engineering*** (Vol. 8, Issue 4, pp. 1396–1426). American Chemical Society.

(3) Merga, Y., Campbell, B. J., & Rhodes, J. M. (2014). Mucosal barrier, bacteria and inflammatory bowel disease: Possibilities for therapy. ***Digestive Diseases***, ***32***(4), 475–483.

(4) Herath, M., Hosie, S., Bornstein, J. C., Franks, A. E., & Hill-Yardin, E. L. (2020). The Role of the Gastrointestinal Mucus System in Intestinal Homeostasis: Implications for Neurological Disorders. In ***Frontiers in Cellular and Infection Microbiology*** (Vol. 10). Frontiers Media S.A.

(5) Munkholm, M., & Mortensen, J. (2014). Mucociliary clearance: Pathophysiological aspects. ***Clinical Physiology and Functional Imaging***, ***34***(3), 171–177.

(6) Umeki, S., & Manabe, T. (1992). [Structure, function and pathophysiology of mucociliary transport system]. ***Nihon Rinsho. Japanese Journal of Clinical Medicine***, ***50***(4), 892–899.

(7) Zhang, J., Wu, L., Chan, H. K., & Watanabe, W. (2011). Formation, characterization, and fate of inhaled drug nanoparticles. In ***Advanced Drug Delivery Reviews*** (Vol. 63, Issue 6, pp. 441–455).

(8) di Berardino, F., Zanetti, D., & D'Amato, G. (2017). Nasal rinsing with an atomized spray improves mucociliary clearance and clinical symptoms during peak grass pollen season. ***American Journal of Rhinology and Allergy***, ***31***(1), 40–43.

(9) del Donno, M., Bittesnich, D., Chetta, A., Olivieri, D., & Lopez-Vidriero, M. T. (2000). The effect of inflammation on mucociliary clearance asthma: An overview. In ***Chest*** (Vol. 118, Issue 4, pp. 1142–1149).

(10) Laucirica, D. R., Garratt, L. W., & Kicic, A. (2020). Progress in Model Systems of Cystic Fibrosis Mucosal Inflammation to Understand Aberrant Neutrophil Activity. In ***Frontiers in Immunology*** (Vol. 11). Frontiers Media S.A.

(11) Baumgart, D. C., & Carding, S. R. (2007). Gastroenterology 1 Infl ammatory bowel disease: cause and immunobiology. In ***www.thelancet.com*** (Vol. 369).

(12) Hejjaji, E. M. A., Smith, A. M., & Morris, G. A. (2018). Evaluation of the mucoadhesive properties of chitosan nanoparticles prepared using different chitosan to tripolyphosphate (CS:TPP) ratios. ***International Journal of Biological Macromolecules***, ***120***, 1610–1617.

(13) Vasquez-Martínez, N., Guillen, D., Moreno-Mendieta, S. A., Sanchez, S., & Rodríguez-Sanoja, R. (2023). The Role of Mucoadhesion and Mucopenetration in the Immune Response Induced by Polymer-Based Mucosal Adjuvants. ***Polymers***, ***15***(7), 1615.

(14) Boegh, M., Foged, C., Müllertz, A., & Mørck Nielsen, H. (2013). Mucosal drug delivery: Barriers, in vitro models and formulation strategies. In ***Journal of Drug Delivery Science and Technology*** (Vol. 23, Issue 4, pp. 383–391). Editions de Sante.

(15) Bandi, S. P., Bhatnagar, S., & Venuganti, V. V. K. (2021). Advanced materials for drug delivery across mucosal barriers. In ***Acta Biomaterialia*** (Vol. 119, pp. 13–29). Acta Materialia Inc.

(16) Laffleur, F., & Bernkop-Schnürch, A. (2013). Strategies for improving mucosal drug delivery. In ***Nanomedicine*** (Vol. 8, Issue 12, pp. 2061–2075). Future Medicine Ltd.

(17) Bhattarai, N., Gunn, J., & Zhang, M. (2010). Chitosan-based hydrogels for controlled, localized drug delivery. In ***Advanced Drug Delivery Reviews*** (Vol. 62, Issue 1, pp. 83–99).

(18) Boylan, N. J., Suk, J. S., Lai, S. K., Jelinek, R., Boyle, M. P., Cooper, M. J., & Hanes, J. (2012). Highly compacted DNA nanoparticles with low MW PEG coatings: In vitro, ex vivo and in vivo evaluation. ***Journal of Controlled Release***, ***157***(1), 72–79.

(19) Bhumkar, D. R., & Pokharkar, V. B. (2006). Studies on Effect of pH on Cross-linking of Chitosan With Sodium Tripolyphosphate: A Technical Note.

(20) Ways, T. M. M., Lau, W. M., & Khutoryanskiy, V. v. (2018). Chitosan and its derivatives for application in mucoadhesive drug delivery systems. In ***Polymers*** (Vol. 10, Issue 3). MDPI AG.

(21) Veronese, F.M., Pasut, G. (2005). PEGylation, successful approach to drug delivery. In ***Drug Discovery Today*** (Vol. 10, Issue 21, pp. 1451-1458).

(22) Knop, K., Hoogenboom, R., Fischer, D., & Schubert, U. S. (2010). Poly(ethylene glycol) in drug delivery: Pros and cons as well as potential alternatives. In ***Angewandte Chemie - International Edition*** (Vol. 49, Issue 36, pp. 6288–6308).

(23) Chen, J., Spear, S. K., Huddleston, J. G., & Rogers, R. D. (2005). Polyethylene glycol and solutions of polyethylene glycol as green reaction media. In ***Green Chemistry*** (Vol. 7, Issue 2, pp. 64–82). Royal Society of Chemistry.

(24) Lai, S. K., Elizabeth O'hanlon, D., Harrold, S., Man, S. T., Wang, Y.-Y., Cone, R., & Hanes, J. (2007). Rapid transport of large polymeric nanoparticles in fresh undiluted human mucus.

(25) Huckaby, J. T., & Lai, S. K. (2018). PEGylation for enhancing nanoparticle diffusion in mucus. In ***Advanced Drug Delivery Reviews*** (Vol. 124, pp. 125–139). Elsevier B.V.

(26) Leiro, P. (2022). Nanopartículas de quitosano y fosvitina. Caracterización y aplicaciones en la industria alimentaria.

(27) Divya, K., & Jisha, M. S. (2018). Chitosan nanoparticles preparation and applications. In ***Environmental Chemistry Letters*** (Vol. 16, Issue 1, pp. 101–112). Springer Verlag.

(28) de Carvalho, F. G., Magalhães, T. C., Teixeira, N. M., Gondim, B. L. C., Carlo, H. L., dos Santos, R. L., de Oliveira, A. R., & Denadai, Â. M. L. (2019). Synthesis and characterization of TPP/chitosan nanoparticles: Colloidal mechanism of reaction and antifungal effect on C. albicans biofilm formation. ***Materials Science and Engineering C***, *104*.

(29) Pan, C., Qian, J., Zhao, C., Yang, H., Zhao, X., & Guo, H. (2020). Study on the relationship between crosslinking degree and properties of TPP crosslinked chitosan nanoparticles. ***Carbohydrate Polymers***, ***241***.

(30) Cadar, D., Manea, D. L., Jumate, E., Popa, F., Moldovan, D., & Fechete, R. (2023). Structural and dynamic characterization of two-component waterproof mortars by 1H NMR, FT-IR, mechanical and SEM investigations. ***Construction and Building Materials***, ***378***.

(31) Najafabadi, A. H., Abdouss, M., & Faghihi, S. (2014). Synthesis and evaluation of PEG-O-chitosan nanoparticles for delivery of poor water soluble drugs: Ibuprofen. ***Materials Science and Engineering C***, ***41***, 91–99.

(32) Huang, M., Khor, E., & Lim, L.-Y. (2004). Uptake and Cytotoxicity of Chitosan Molecules and Nanoparticles: Effects of Molecular Weight and Degree of Deacetylation. (30)

(33) Kou, S. (Gabriel), Peters, L. M., & Mucalo, M. R. (2021). Chitosan: A review of sources and preparation methods. In ***International Journal of Biological Macromolecules*** (Vol. 169, pp. 85–94). Elsevier B.V.

(34) Nguyen, S., Hisiger, S., Jolicoeur, M., Winnik, F. M., & Buschmann, M. D. (2009). Fractionation and characterization of chitosan by analytical SEC and 1H NMR after semi-preparative SEC. ***Carbohydrate Polymers***, ***75***(4), 636–645. (35)

(35) Rampino, A., Borgogna, M., Blasi, P., Bellich, B., & Cesàro, A. (2013). Chitosan nanoparticles: Preparation, size evolution and stability. ***International Journal of Pharmaceutics***, ***455***(1–2), 219–228.

(36) Fan, W., Yan, W., Xu, Z., & Ni, H. (2012). Formation mechanism of monodisperse, low molecular weight chitosan nanoparticles by ionic gelation technique. ***Colloids and Surfaces B: Biointerfaces***, ***90***(1), 21–27.

(37) Zhang, H., Bahamondez-Canas, T. F., Zhang, Y., Leal, J., & Smyth, H. D. C. (2018). PEGylated Chitosan for Nonviral Aerosol and Mucosal Delivery of the CRISPR/Cas9 System in Vitro. ***Molecular Pharmaceutics***, ***15***(11), 4814–4826.

(38) Kholodenko, A. L., & Douglas, J. F. (1995). ***PACS number(s): 66.20. +d, 61.25. Hq, 64.60.Ht, 46.30*** (Vol. 51, Issue 2).

(39) Udabe, J. (2020). Nanoparticle mediated siRNA delivery system for skin disorders

(40) Bhattacharjee, S. (2016). DLS and zeta potential - What they are and what they are not? In ***Journal of Controlled Release*** (Vol. 235, pp. 337–351). Elsevier B.V.

(41) Malvern Instruments (n.d.). Dynamic Light Scattering: An Introduction in 30 Minutes.

(42) Gruber, A., Işik, D., Fontanezi, B. B., Böttcher, C., Schäfer-Korting, M., & Klinger, D. (2018). A versatile synthetic platform for amphiphilic nanogels with tunable hydrophobicity. ***Polymer Chemistry***, ***9***(47), 5572–5584.

(43) Fonte, P., Reis, S., & Sarmento, B. (2016). Facts and evidences on the lyophilization of polymeric nanoparticles for drug delivery. In ***Journal of Controlled Release*** (Vol. 225, pp. 75–86). Elsevier B.V.

(44) Vandana, M., & Sahoo, S. K. (2009). Optimization of physicochemical parameters influencing the fabrication of protein-loaded chitosan nanoparticles. ***Nanomedicine***, ***4***(7), 773–785.

(45) Tanasi, D., Greco, E., di Tullio, V., Capitani, D., Gullì, D., & Ciliberto, E. (2017). 1H-1H NMR 2D-TOCSY, ATR FT-IR and SEM-EDX for the identification of organic residues on Sicilian prehistoric pottery. ***Microchemical Journal***, ***135***, 140–147.

(46) Udabe, J. (2019). Incorporación de sales de zinc en recubrimientos sol-gel para implantes dentales.

(47) Puviarasan, N., Arjunan, V., & Mohan, S. (2002). FT-IR and FT-Raman Studies on 3-Aminophthalhydrazide and N-Aminophthalimide. ***Turkish Journal of Chemistry*** (Vol. 26, Issue 3).

(48) Thygesen, L. G., Løkke, M., Micklander, E., & Engelsen, S. B. (2003). Vibrational microspectroscopy of food. Raman vs. FT-IR.

(49) Wetzel, D.L. & LeVine, S.M. (1999). Imaging Molecular Chemistry with Infrared Microscopy. ***Science's Compass*** (Vol. 285, pp. 1224-1225).

(50) Koenig, J. L., & Antoon, M. K. (1978). Recent applications of FT-IR spectroscopy to polymer systems. ***Applied Optics, 17***(9), 1374-1385.

(51) Fabian, H., & Naumann, D. (2004). Methods to study protein folding by stopped-flow FT-IR. ***Methods***, ***34***(1), 28–40.

(52) Cappella, B., & Dietler, G. (1999). Force-distance curves by atomic force microscopy. ***Surface Science Reports, 34,*** 1-104.

(53) Eftink, M. R. (2002). Fluorescence Quenching: Theory and Applications. ***Topics in Fluorescence Spectroscopy, 2,*** 53-126.

(54) Barbero, N., Coletti, M., Catalano, F., & Visentin, S. (2018). Exploring gold nanoparticles interaction with mucins: A spectroscopic-based study. ***International Journal of Pharmaceutics***, ***535***(1–2), 438–443.